Eur Biophys J
DOI 10.1007/s00249-015-1080-3

ORIGINAL PAPER

Unit cell structure of water-filled monoolein in inverted hexagonal mesophase in the presence of incorporated tricaprylin and entrapped lysozyme

Vesselin Kolev[1,2] · Anela Ivanova[3] · Galia Madjarova[3] · Abraham Aserin[4] · Nissim Garti[5]

Received: 20 June 2015 / Revised: 1 September 2015 / Accepted: 2 September 2015

Abstract Molecular dynamics (MD) was employed by means of a specific simulation protocol to investigate the equilibrium structure at 25 °C of the hexagonal inverted (H_{II}) mesophase composed from water, 1-monoolein (GMO), and tricaprylin, with or without entrapped lysozyme. Based on robust and fast MD simulations, the study provides a comprehensive analysis and visualization of the local structure of H_{II} mesophase containing admixtures. The most important physical insight is the possibility to observe the strong self-recovery capacity of the GMO layer, which allows the H_{II} mesophase tubes to reorganize and host lysozyme molecules with a size bigger than the diameter of the water channel. This is a direct message to the experimenters that the H_{II} mesophase has the potential to host molecules larger than the diameter of the water channel. Collective character of the interlipid interactions is outlined, which is not affected by the presence of the cargo and may be the reason for the efficient GMO reorganization. Another important result is the possible explanation of the role of triacylglycerols on the low-temperature stabilization of the H_{II} mesophase. The analysis shows that despite the low amount of tricaprylin, its molecules prevent the extreme inclination of the lipid tails and thus optimize the alignment capacity of the lipid tails layer. The study also reveals that the packing frustration does not depend on the temperature and the presence of admixtures. Hence, it might be numerically defined as a universal invariant parameter of a stable H_{II} mesophase composed of a certain lipid.

Keywords Monoolein · Inverted hexagonal (H_{II}) mesophase · Tricaprylin · Lysozyme · Molecular dynamics · Mass density distribution maps

Electronic supplementary material The online version of this article (doi:10.1007/s00249-015-1080-3) contains supplementary material, which is available to authorized users.

✉ Vesselin Kolev
vlk@lcpe.uni-sofia.bg

[1] The Wolfson Department of Chemical Engineering, Technion, Technion City, 32000 Haifa, Israel

[2] Department of Chemical Engineering, Faculty of Chemistry and Pharmacy, Sofia University "St. Kliment Ohridski", 1 James Bourchier Blvd., Sofia 1164, Bulgaria

[3] Department of Physical Chemistry, Faculty of Chemistry and Pharmacy, Sofia University "St. Kliment Ohridski", 1 James Bourchier Blvd., Sofia 1164, Bulgaria

[4] The Institute of Chemistry, The Hebrew University of Jerusalem, Edmond J. Safra Campus, Givat Ram, 91904 Jerusalem, Israel

[5] The Ratner Chair in Chemistry, Casali Institute of Applied Chemistry, The Institute of Chemistry, The Hebrew University of Jerusalem, Edmond J. Safra Campus, Givat Ram, 91904 Jerusalem, Israel

Introduction

The lyotropic liquid crystals of glycerol monooleate (1-monoolein, GMO) are involved in phase transitions from lamellar (L_α) or cubic (Q) to inverted (reverse) hexagonal mesophase at about 70 °C (Kulkarni et al. 2011; Alfutimie et al. 2015). Some of the physical and chemical properties of GMO in the H_{II} mesophase render this system a possible supplier of cargo molecules into biological systems. However, this potential is exploitable only if the temperature of the phase transition can be decreased to the one in vivo. It has been reported recently that the incorporation of triacylglycerols (TAGs) in the GMO-based lyotropic liquid crystals lowers the temperature of the phase transitions and it

Published online: 30 September 2015

is possible to have H_{II} mesophase at temperature as low as 25 °C (Amar-Yuli and Garti 2005). Several experimental studies at that temperature show the ability of the GMO-based H_{II} mesophase with incorporated TAG to entrap biologically active molecules (Libster et al. 2007; Fehér et al. 2008; Efrat et al. 2008; Mishraki et al. 2010a, b; Amar-Yuli et al. 2011; Libster et al. 2011; Zabara and Mezzenga 2012; Aherne et al. 2012). For example, a spectroscopic investigation was performed on hexagonal inverted mesophase assembled from GMO, water, and tricaprylin, where lysozyme was entrapped by solubilization (Mishraki et al. 2010a, b; Zabara et al. 2011; Zabara and Mezzenga 2013). It was seen that upon increase of the lysozyme amount, the smallest GMO tubes expand slightly but are soon disintegrated, while the larger ones remain stable after higher peptide uptake (up to weight fraction 0.035 in the widest tube). Moreover, the tubes with higher lattice parameter shrink after lysozyme insertion.

The observed decrease of the phase transition temperature due to TAGs inclusion and the ability of the mesophase to entrap biologically active molecules raise at least two significant questions. The first is related to the structure of the H_{II} mesophase with incorporated TAG molecules. It is important to know if TAG and GMO molecules are just interspersed or if the TAG molecules have specific positions with respect to the GMO–water interface. The second question is about the process of lysozyme entrapment—where the lysozyme molecules are located in the GMO tubes, how they modify the structure of the tubes they are entrapped in, and how the peptide molecule is affected by the entrapment. Up to now, the answers could not be provided by the experimental methods applied for structural investigation. For example, the electronic density maps from XRD do not reveal the longitudinal structure of the tubes and in the latitudinal direction, which can be visualized by XRD, not enough details can be discerned. Also, it is not possible to plot separate maps for each of the components (GMO, water, TAG, or lysozyme).

An alternative elucidation of the local structure of the H_{II} mesophase with included TAG and entrapped lysozyme is feasible through the methods of molecular dynamics (MD), which can be employed to model the tube structure. The pioneer MD studies of Marrink and Tieleman predicted both the structure of a particular mesophase and the conditions for phase transitions. Their simulation protocol is very realistic and allows investigation of both the lipid self-assembly and the phase transitions within relatively short (50–60 ns) simulations. The experimental method of reconstructed electron density maps (Di Gregorio and Mariani 2005) confirms not only their simulation results for the H_{II} mesophase but also the validity of mechanical models like the tilt model of (Hamm and Kozlov 1998). Inspired by that success, we have designed and successfully implemented in our previous studies (Kolev et al. 2012, 2014) a new fast construction protocol for the H_{II} mesophase of single-tailed lipids. It generates an initial structure of the mesophase tube based on experimental data and easily equilibrates it by running relatively short (less than 50 ns) NVT MD simulations (Kolev et al. 2014). The major physical insight of the protocol is the possibility to observe the local features of the H_{II} mesophase structure along and across the tube in great detail, and precisely obtain the shape (topology) and thickness of GMO tails layer and GMO–water interface. The NVT ensemble is naturally employed (Kolev et al. 2014) because of the experimentally observed large and well-defined-in-shape crystals of H_{II} tubes, which enables a numerical fit of the model to the lattice parameter of the crystal. In order to prove that the adopted combination of proposed initial structure and NVT simulations does not create artifacts, mechanical stress, or entrap the system into a local potential/total energy minimum, we ran NPT simulations in parallel (Kolev et al. 2014). The comparison of the results proved that our simulation protocol is capable of producing a relaxed H_{II} structure that samples profoundly the thermodynamically accessible phase space (Kolev et al. 2014).

In the current work, the model is improved to the next level, namely, introducing tricaprylin and lysozyme into the initial GMO–water system without causing structural congestions that may affect the mechanical balance and create artifacts compromising the equilibration simulation. One goal is to assess the role of the tricaprylin in the stabilization of the H_{II} mesophase at low temperature. Next, we need to answer the question why lysozyme cannot cut the tubes with diameter of the water cylinder smaller than the size of the peptide itself. However, the most important question within this study is whether the SAXS spectroscopic fingerprints for the H_{II} mesophase (Kulkarni et al. 2011) may in all cases be predicted by simple classical structural models.

Models and methods

Molecular chemical structures and force field

The molecular structures of 1-monoolein, tricaprylin, and lysozyme are drawn in Fig. 1.

The force field CHARMM27 (Klauda et al. 2005; Feller and MacKerell 2000) was employed to supply the interaction parameters for the organic molecules and TIP3P—for water. The routine RESP (Bayly et al. 1993; Cieplak et al. 1995) was used to calculate the atomic charges of GMO and tricaprylin given in Section S1 of the Supplementary Material.

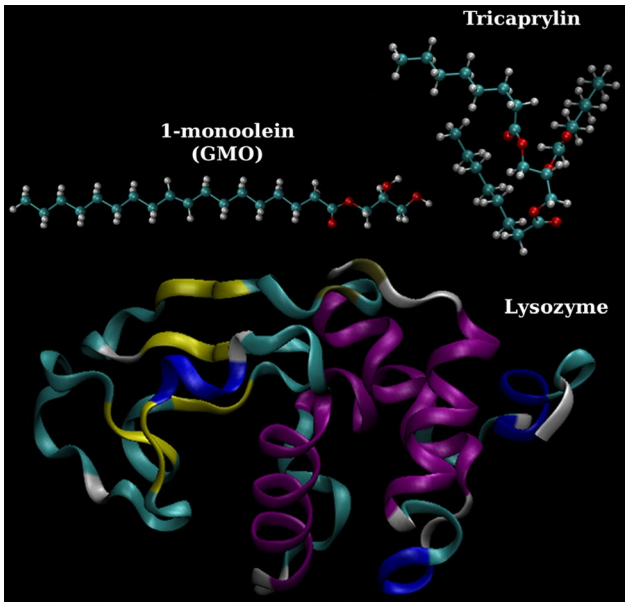

Fig. 1 Sketch of the molecular structures of GMO (M_G = 356.55 a.m.u.), tricaprylin (M_T = 470.69 a.m.u.), and lysozyme (M_L = 14,313.18 a.m.u.) involved in the molecular dynamics simulations. The lysozyme structure is the one with PDB ID 1AKI in the Protein Data Bank; *different colors* correspond to a different secondary structure (Artymiuk et al. 1982); details about the peptide are given in Section S2 of the Supplementary Material. All molecular structures are visualized by using VMD (Humphrey et al. 1996)

Assembly of the simulation boxes in accordance with experiment

The experimentally measured lattice parameter of the H_{II} mesophase, α, the length of each box (tube), L, and the weight ratios of water, GMO, tricaprylin, and lysozyme (if present) are supplied by Fig. S3 of Section S3 of the Supplementary Material. The non-zero charge (+8e) when lysozyme is present is neutralized by adding 10 Na^+ and 18 Cl^- ions in the water for proper screening of the charged amino acid residues.

Table 1 provides the calculated amount of molecules and ions in each simulation box. The corresponding box sizes (the unit vectors) are given in Section S4 of the Supplementary Material (Table S3).

An extended version of the assembly routine developed previously (Kolev et al. 2014), implemented as a set of modules written by one of the authors in Python 2.7 with support of SQLite 3.6.20 and HDF5, draws the molecular coordinates of the initial structures of the mesophase, as illustrated in Fig. 2. The tricaprylin molecules are placed at the end of the GMO tails to prevent structural congestion that may hamper the potential energy minimization. Their position relative to the center of mass is calculated based on the same lattice routine adopted for the initial positioning of the GMO headgroups (see Fig. S3 in the Supplementary Material of Ref. Kolev et al. 2014). In order to avoid overlap of the GMO molecules with the lysozyme, which may cause the energy minimizer to fail, the GMO tube is divided into two parts to make room for hosting the lysozyme molecule (Fig. 2b). Such an initial division of the tube leads to compression of the GMO layer but it is easily resolved later during the energy minimization so no artifacts of that process remain in the structure. Also due to that way of placing the lysozyme, during the equilibration, the GMO molecules fit closely to the lysozyme molecule and thus help in establishing equilibrium faster.

Periodic boundary conditions (PBC) are introduced to represent an infinite H_{II} mesophase in all calculations.

Simulation protocol

Each simulation box described in Table 1 is subject to a standard multistage MD simulation protocol described in details (incl.

Table 1 Quantitative description of the simulation boxes obtained by means of the formulas in Section S4 of the Supplementary Material using the experimental data from Ref. Mishraki et al. (2010a, b) (also plotted in Fig. S3 of the Supplementary Material)

R_w (Å)	α (Å)	L (Å)	N_W	N_G	N_T	N_L	N_{Na^+}	N_{Cl^-}	Atoms
Without entrapped lysozyme									
8.73	47.32	200	1598	486	41	0	0	0	39,787
10.94	53.41	200	2509	599	50	0	0	0	50,612
13.16	57.36	200	3627	660	56	0	0	0	58,429
14.32	58.18	200	4298	654	55	0	0	0	59,969
With entrapped lysozyme									
8.84	47.82	1262	10,302	2307	262	1	10	18	204,595
10.81	52.56	523	6371	1491	126	1	10	18	128,474
12.30	53.32	335	5276	929	78	1	10	18	84,675
13.51	54.55	274	5212	760	64	1	10	18	72,336

The first four rows correspond to mesophase with no entrapped lysozyme, while the others quantitatively describe the mesophase with the highest possible content of lysozyme at a given water fraction

The columns contain the lattice parameter (α), the radius of the water cylinder (R_w) (Kolev et al. 2012, 2014), the number of water (N_W), GMO (N_G), tricaprylin (N_T), and lysozyme (N_L) molecules; the number of sodium (N_{Na^+}) and chloride (N_{Cl^-}) ions; and the total number of atoms in each simulation box

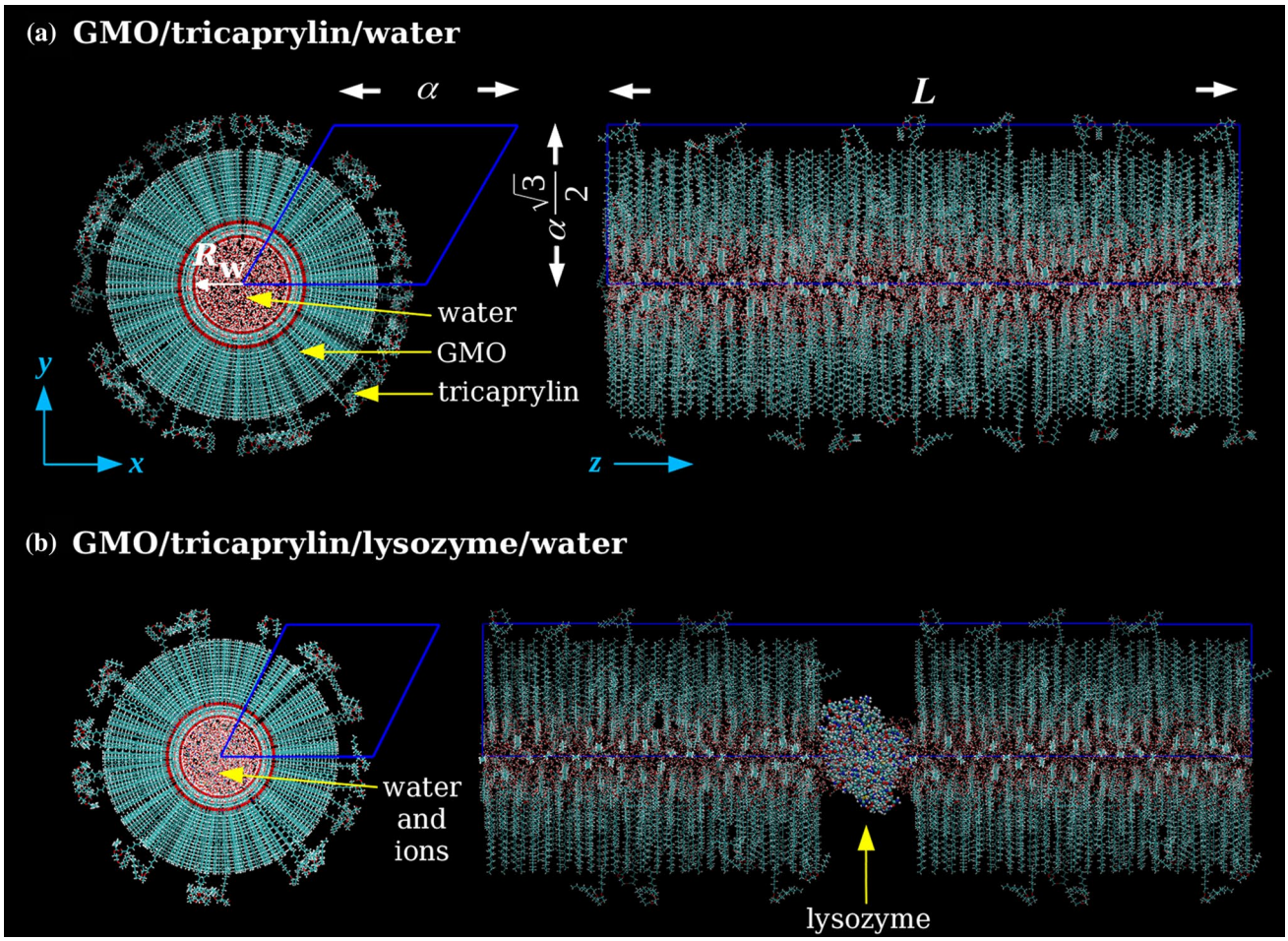

Fig. 2 **a** GMO–tricaprylin–water and **b** GMO–traicaprylin–lysozyme–water initial structure. *Blue lines* are the contours of the simulation box; α, L, and R_w are the lattice parameter, the length of the GMO tube, and the radius of the water cylinder, respectively. The peptide (lysozyme) is depicted with *solid spheres* in **b**

the GROMACS (Bekker et al. 1993; Berendsen et al. 1995; Lindahl et al. 2001; van der Spoel et al. 2005 start configurations) in Section S5 of the Supplementary Material). The productive stage of the simulation is 120 ns long and its trajectory collects frames (atomic coordinates and velocities) at every 1 ps.

The analyses are based on the last 60 ns of each productive stage in order to have identical statistical samples for all systems. Both GROMACS tools set and grid statistics on the atomic mass spatial distribution, described in Section S6 of the Supplementary Material, are used for analysis. The grid statistics is programmed in Python 2.7 and Fortran 2003 (with OpenMP) by one of the authors.

Results and discussion

General notes on the success of the simulation process

After the simulations, all systems (Table 1), except the one with $R_w = 8.84$ Å, match the structural model of a single infinite tube. Figure 3 reveals that the tube with $R_w = 8.84$ Å has a large gap, which is not observed in the other tubes. It should be noted that also the experimentally studied system at 13 wt % water, to which this model corresponds, statistically differs from the one observed for the other systems (Fig. S3 of the Supplementary Material).

Figure 3 is a possible answer to the question raised in the Introduction about the compliance between the SAXS fingerprints for the H_{II} mesophase (Kulkarni et al. 2011) and the actual structure. It shows that the classical formulas in Section S4 of the Supplementary Material, which are derived for long tubes by neglecting the boundary effects on both sides, may fail when the water content is low. One possible explanation of that discrepancy is that the H_{II} mesophase at low water content is composed of a series of tubes with different length (some of them might be as short as emulsion vesicles) so the protrusion at the borders may fill in the gap. If this is the case, the SAXS will still measure a fingerprint of the H_{II} mesophase but the structure of the mesophase might not be the typical one and its properties

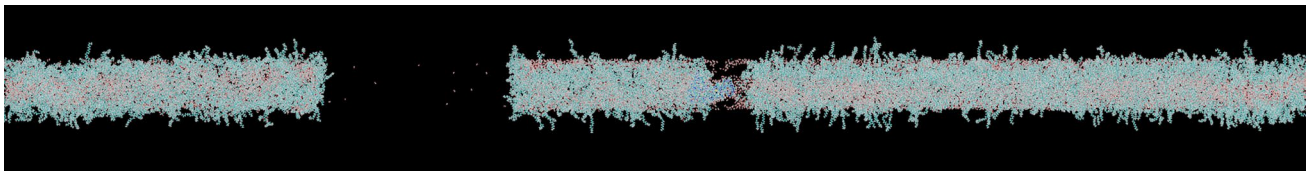

Fig. 3 The rupture of the structure with $R_w = 8.84$ Å during the equilibration. Note that even for 1-μs-long simulation the gap remains, and no structural reconfiguration is detected

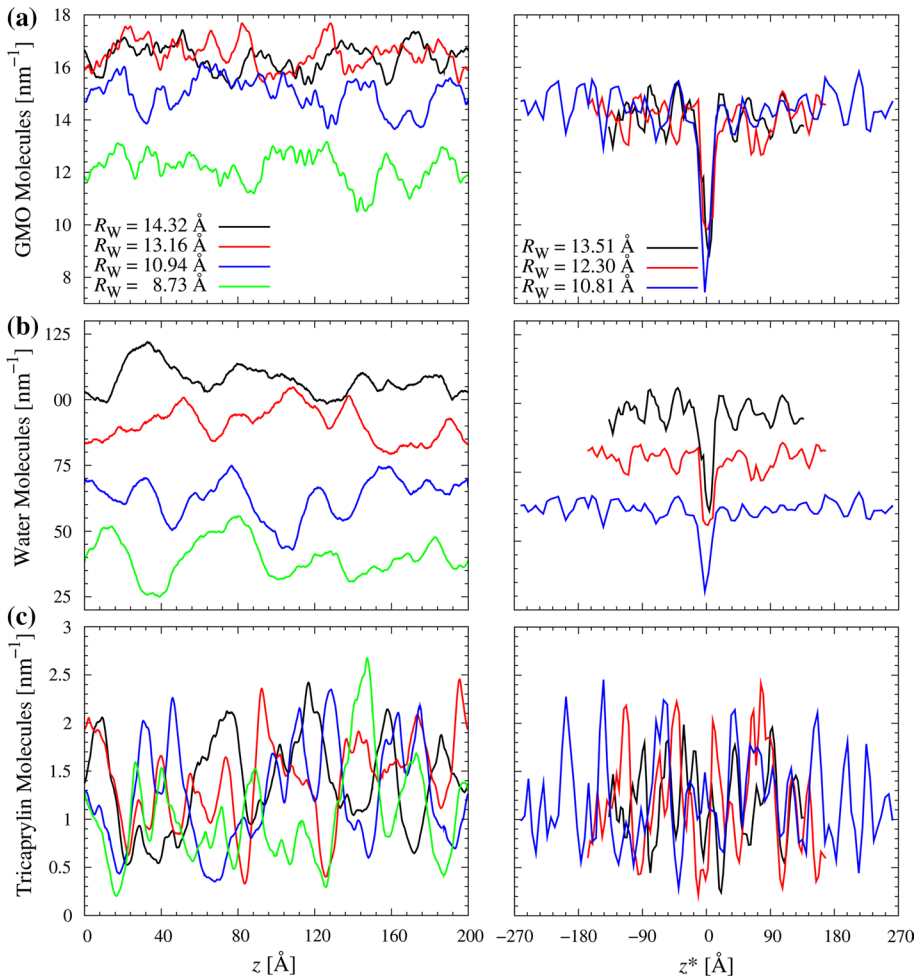

Fig. 4 Distribution of the number of GMO (**a**), water (**b**), and tricaprylin (**c**) molecules along the z-axis of the hexagonal inverted mesophase tube in case of no (*left*) or entrapped lysozyme (*right*). Note that the abscissa for the boxes containing lysozyme is redefined as $z^* \equiv z - L/2$ with respect to the center of mass of the lysozyme molecule (which is at $z^* = 0$), to allow better comparison of the results

cannot be compared to the ones related to the systems with high water content. So, in that case, the structure might be classified as non-typical and transient, which is not covered by the classical structural theories of the H_{II} mesophase and does not obey the model adopted by the analysis routine here. Hence, this model is excluded from further analysis.

Structural analysis based on the atomic mass distribution

Based on the grid statistics routine described in Section S6 of the Supplementary Material, Fig. 4 represents the normalized number of each molecular species along the z-direction (the length) of the H_{II} mesophase tubes.

All plots show fluctuations but their amplitudes along the tubes axis or among the different systems do no*t* correlate. For the tubes with entrapped lysozyme, the fluctuations are much more pronounced and more uniformly distributed at low water content. There, the distance between two lysozyme molecules in the tube is longer and the tube itself is the most flexible along z. At high water content, the lysozyme molecules are much closer, and the structure is more perturbed locally because there is less space to distribute the structural

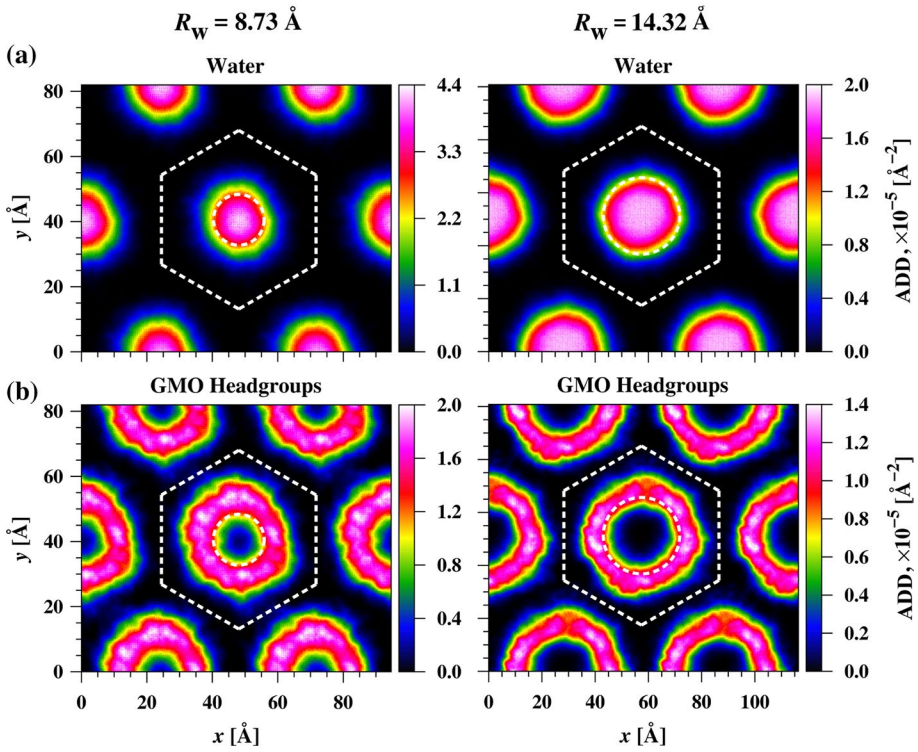

Fig. 5 ADD in latitudinal (*xy*) direction of the simulation box estimated for the atomic mass of water (**a**) and the GMO headgroups (**b**) obtained in the H_{II} mesophase without entrapped lysozyme with the lowest ($R_w = 8.73$ Å) and highest ($R_w = 14.32$ Å) water content described in Table 1. The hexagonal unit cell and the shape of the water cylinder, as predicted by Luzzatti and Husson (Luzzati and Husson 1962), are sketched with *dashed lines*

perturbation caused by insertion of the lysozyme molecule.

Despite the fluctuations, the number of tricaprylin molecules per unit tube length ($\Delta z = 1$ nm) is statistically constant and does not depend on the water content (Fig. 4c). Even the presence of lysozyme does not change (see the right-hand side of Fig. 4c at $z^* \approx 0$).

In order to reveal more of the local structure of the H_{II} mesophase, the distribution of the atomic mass (ADD) at each point of the tube is calculated (Section S6 of the Supplementary Material) and plotted in Figs. 5, 6, 7, 8, S11, and S12. Figure 5 shows the latitudinal (*xy* cross-section) structure of the H_{II} mesophase tubes with incorporated tricaprylin. The water volume (Fig. 5a) has a cylindrical shape and the part of ADD within the >90 % confidence limit fully fits the outer surface of the GMO headgroups layer (Fig. 5b), which indicates complete solvation of the headgroups.

The maximum ADD values for water at low water content are much higher, which means that large share of the water molecules is located close to the center of the cylinder and a relatively small fraction—amid the GMO headgroups (the water density profile is more smeared). Also, unlike the result reported in our previous study at 70 °C (Kolev et al. 2014), the GMO headgroups layer here does not form hexagonal shape. Instead, its shape is close to the one predicted by the classical structural theory developed by Luzzatti and Husson (Luzzati and Husson 1962).

Figure 6 tries to answer the question about the positioning of the incorporated tricaprylin molecules in the structure of the H_{II} mesophase. It appears that they form islands among the GMO molecules. As expected, the larger mass density fraction is positioned among the GMO tails, while only the polar part is close to the GMO headgroups layer. Note that the maximum ADD values in Fig. 6b for the tubes with the lowest and highest water content are almost the same, in accordance with Fig. 4c, which means that the latitudinal distribution of tricaprylin is not governed by the size of the GMO cylinder. Another interesting result of this study that can be compared to the data derived at 70 °C in our previous study (Kolev et al. 2014) can be seen in Fig. 6a. There, the GMO tails are homogeneously distributed along the entire cross-sectional area of the tubes, whereas in the absence of tricaprylin [70 °C (Kolev et al. 2014)] there was clear GMO density enhancement at the hexagon vertices. This could be explained as follows: at 70 °C a single most probable conformation of the GMO tails was detected. It rendered almost constant tails length and the GMO–water interface would fit the hexagonal shape of the tails layer. At 25 °C the upper parts of the GMO tails become grouped at the vertices of the unit cell (Fig. S11 of the Supplementary Material). However, no such dominant conformation of the GMO tails is detected at the lower temperature (see below). So, it is likely that at this temperature the remaining part of the tails compensates conformationally to result in different overall tails distribution. Complete investigation of that effect, however,

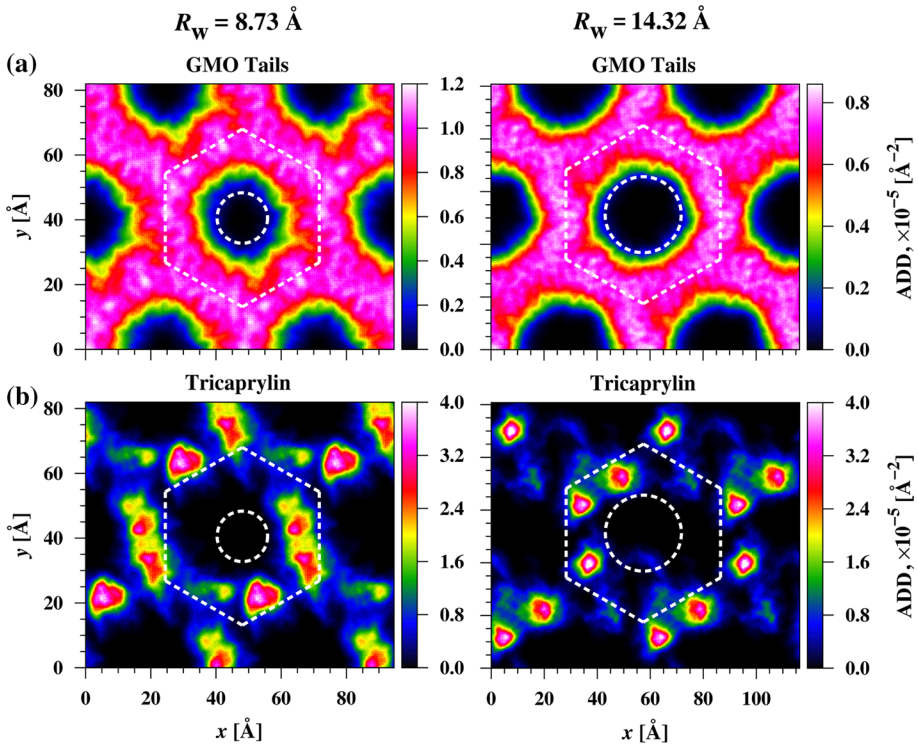

Fig. 6 ADD in latitudinal (*xy*) direction of the simulation box estimated for the atomic mass of the GMO tails (**a**) and tricaprylin (**b**), obtained in the H_{II} mesophase without entrapped lysozyme with the lowest ($R_w = 8.73$ Å) and highest ($R_w = 14.32$ Å) water content described in Table 1. The hexagonal unit cell and the shape of the water cylinder, as predicted by Luzzatti and Husson (Luzzati and Husson 1962), are sketched with *dashed lines*

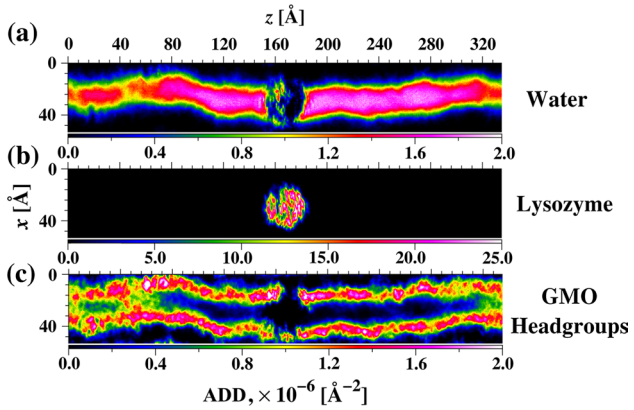

Fig. 7 The longitudinal ADD of water (**a**), the entrapped lysozyme (**b**), and the GMO headgroups (**c**) in the H_{II} mesophase with content corresponding to $R_w = 12.30$ Å (see Table 1). Note that the plotted phenomena appear in almost the same quality and quantity in the H_{II} mesophase with $R_w = 52.56$ Å and $R_w = 13.51$ Å. See Section S6.5 and Fig. S10 in Supplementary Material for more information about the derivation of the plotted maps

is beyond the scope of the study. It can only be suggested that this is in support of the idea that the molecules of tricaprylin occupy positions that enable more efficient and more homogeneous overall packing of the lipid molecules. As a result, the thermodynamically more stable cylindrical shape of the tube channels is observed.

The longitudinal atomic mass distribution of the systems GMO–tricaprylin–water is discussed in Section S7 of the Supplementary Material. Figures 7 and 8 give details on how the inverted hexagonal (H_{II}) mesophase entraps the lysozyme molecules. The longitudinal analysis of the atomic mass plotted in Fig. 7 shows that the lysozyme molecule (Fig. 7b) discontinues the water profile along the tube channel (Fig. 7a), which should affect both the mobility of water molecules and the hydration of the GMO headgroups. Also, it is well visible that the entrapped peptide suppresses the formation of the GMO headgroups layer (Fig. 7c) by filling almost the entire tube space and in one region protruding also out of the water channel (see Fig. S10 of the Supplementary Material). It should be noted, however, that the mass distribution of GMO around the peptide never reaches zero; hence, there is no permanent rupture of the tube. Since the position of the entrapped lysozyme molecule that affects the H_{II} mesophase tube is seen in Fig. 7, it is possible to plot latitudinal ADD of the components around that position and extend the analysis. As shown in Fig. 8, such analysis is more informative than the one based on Fig. 7.

Figure 8a, b can be used to discern the latitudinal hydration profile of the peptide. The water profile is virtually continuous around the peptide with some enhancement in the upper left part, which probably corresponds to a surface hydrophilic fragment of lysozyme. A substantial part of the water distribution also overlaps with that of the peptide, which stems mainly from the part of the tube (in axial dimension) not populated by the peptide. However, there are three more pronounced voids in the water latitudinal

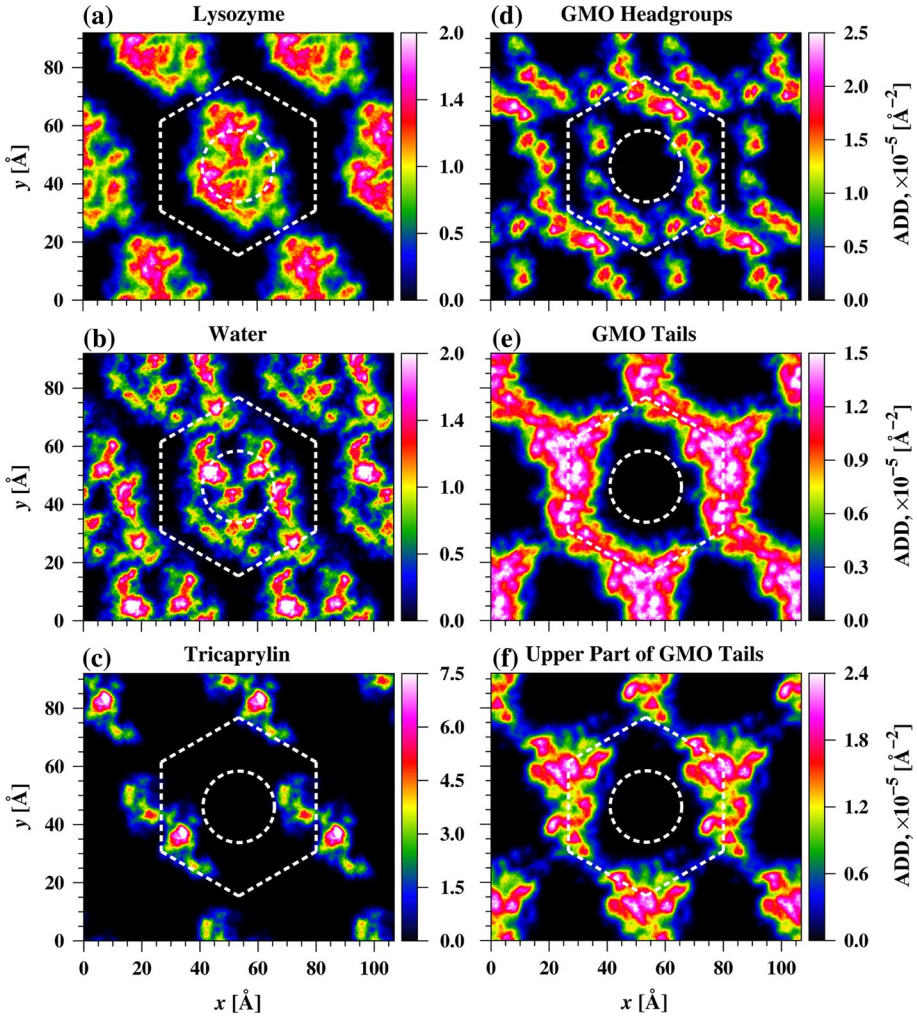

Fig. 8 Latitudinal atomic mass distribution of the entrapped lysozyme (**a**), water (**b**), incorporated tricaprylin (**c**); and the GMO headgroups (**d**), tails (**e**), and upper part of the tails (**f**) as components of the H_{II} mesophase with $R_w = 12.30$ Å (see Table 1). The cross section of the water cylinder with radius R_w (predicted by the theory of Luzzati and Husson 1962) and the shape of the unit cell are sketched with *dashed lines*

distribution. The largest one maps onto a very dense part of the peptide and it may be concluded that the access of water is spatially restricted there. The other two coincide with less dense regions of the peptide. It can be assumed that these are expressed hydrophobic surfaces of lysozyme from which water is repelled. Thus, the plotted density profiles may serve as guidelines for the surface specificity of the peptide.

Figure 8e shows that the H_{II} mesophase entraps lysozyme in a shell, which is thinned out by the peptide only at certain places but not enough to destroy the tube. It is evident that wherever the density of GMO tails becomes close to zero, this thinning is compensated by denser packing of the headgroups and vice versa. This implies certain inclination of the GMO molecules, which is analyzed in the next section.

Axial inclination of GMO tails

Figure 9 presents the definition of the angle θ, which is suggested as a numerical estimator of the axial inclination of the GMO tails. The distribution of θ determined from the molecular dynamics trajectories is plotted in Fig. 10.

The inflection point of each curve there, θ_{infl}, corresponds to the critical inclination above which the GMO tails are expected to participate mainly in axial tail–tail interactions. Such interactions indicate disorder of the GMO tail layer that brings destabilization to the mesophase structure. Note that the inflection points scattering in Fig. 10 shows no correlation with the water (or GMO) content, which is due to the fact that it falls within the statistical error bars. It is not a surprise that the GMO tails predominantly populate the smaller angles, because it reflects an orientation normal to the tube axis and tighter packing of the lipids. The presence of tricaprylin molecules also prevents the GMO tails from populating too much the highest θ. Nevertheless, there is sizable probability of all axial inclination angles. This shows that part of the lipids are disordered and no regular lattice is formed.

Removing just 1 % of the tricaprylin molecules has a sizeable effect on the axial inclination angle distribution (Fig. 10a, dashed lines). In all models, the population of the

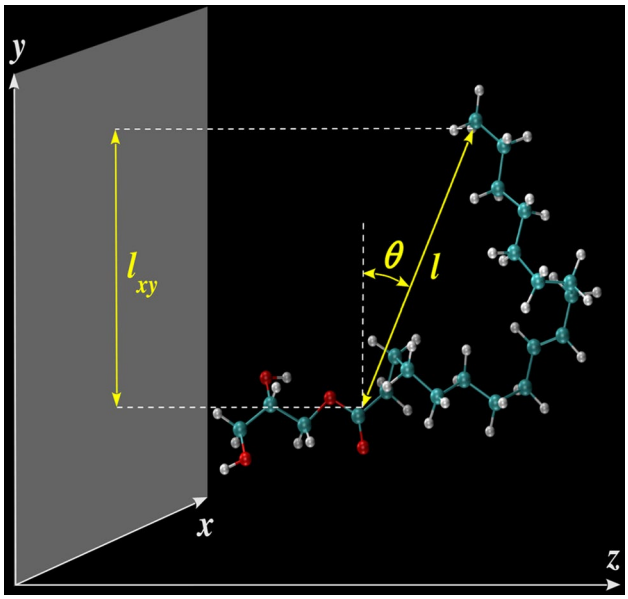

Fig. 9 The maximum length of the GMO tail, l, its projection onto the xy-plane, l_{xy}, and the axial inclination angle, θ. Here, l is defined as the maximum distance that can be measured between the last carbon atom of the GMO headgroup and a carbon atom in the tail (not necessarily the outermost one)

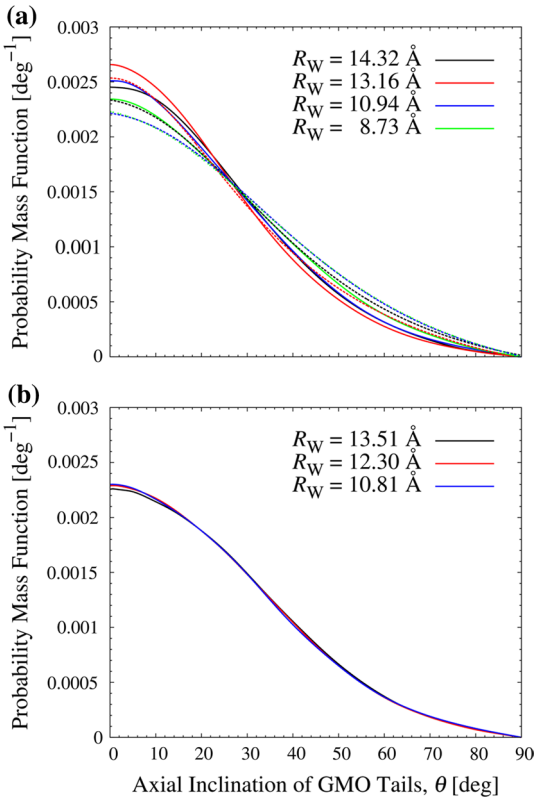

Fig. 10 Distribution of the axial inclination angle of the GMO tails, θ (see Fig. 9 for definition) measured for H_{II} mesophase incorporating tricaprylin without (**a**) and with (**b**) entrapped lysozyme. The histograms are normalized by dividing each measurement to the sum of all measurements. *Dashed lines* in **a** result from perturbed simulations with 1 % less tricaprylin and illustrate its influence on the tubes structure

smallest angles decreases at the expense of the larger values. This confirms the fact that tricaprylin aids tighter packing of the lipid tail layer.

The presence of lysozyme (Fig. 10b) leads to identical distribution of the GMO axial inclinations in all tubes eliminating even the mild influence of the tube diameter. The angle profiles become broader with more populated larger θ. This may be interpreted as a slightly increased level of disorder, which is caused by the peptide interrupting the continuity of the GMO layers.

Packing frustration analysis

Figure 11 introduces the distribution of the parameters, which was employed to analyze the packing frustration effect on the GMO tails. The statistical analysis is an extended version of the one we used before (l is the new parameter here) (Kolev et al. 2014). It investigates the distributions of l_{xy} and l to assess the thickness of the GMO tail layer, which is a quantitative measure of the packing frustration effect. Table 2 provides the numerical results.

If the effect of packing frustration exists in the xy-direction, the average thickness of the GMO tail layer, $\langle \Delta l_{xy} \rangle$ (obtained as the average distance between the inflection points of the l_{xy} curves in Fig. 11) should be very close to the absolute tail frustration estimator $\langle \Delta l \rangle$, which is independent of the projection. According to Table 2, the difference $\langle \Delta l_{xy} \rangle - \langle \Delta l \rangle$ is about 0.5–0.6 Å, and therefore the packing frustration effect is clearly pronounced even for the relatively short simulation boxes. Note that the effect is slightly better expressed in the H_{II} mesophase with no entrapped lysozyme. The difference between $\langle \Delta l_{xy} \rangle$ and $\langle \Delta l \rangle$ is due to the bending of the water channel, so it is a numerical estimator of that effect. The same difference can be obtained numerically by analyzing the direction of fluctuation of the unit vector normal to the transversal intersection of the water channel. If the results in Table 2 are compared to the ones reported in our previous study at 70 °C (Kolev et al.), $\langle \Delta l \rangle$ ought to be related to the Δl_c published there. Such a comparison shows that $\langle \Delta l \rangle$ and Δl_c are statistically indistinguishable, which means that the temperature and presence of admixtures does not change significantly the frustration of GMO tails layer. Therefore, $\langle \Delta l \rangle$ should be considered an invariant structural parameter of the H_{II} mesophase. Figure 6a also shows that the frustration creates a layer of GMO tails, the thickness of which along the structure profile projected onto the xy plane is a constant, even at the unit cell vertices. However, the GMO tails

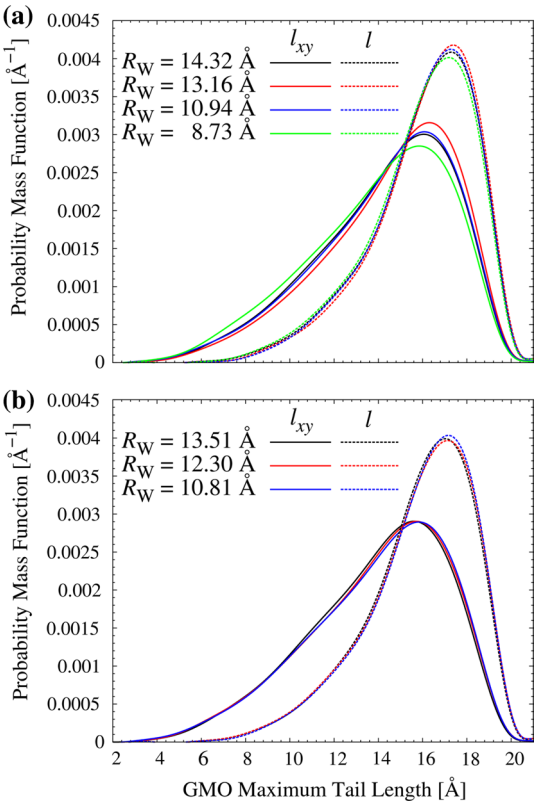

Fig. 11 Distribution of two- (l_{xy}) and three-dimensional (l) maximal GMO tail length (defined in Fig. 9), estimated for H_{II} mesophase incorporating tricaprylin without (**a**) and with (**b**) entrapped lysozyme. The normalization used for Fig. 10 is applied. Note that the abscissa corresponding to the curves maximum for l gives the actual thickness of the GMO tails layer, l_t

layer thickness, l_t, here is not equal to that at 70 °C (Kolev et al. 2014), due to the well pronounced axial inclination at 25 °C (see "Axial inclination of GMO tails").

Ordering of GMO molecules

The parameters discussed so far provide more global characterization of the lipids distribution in the H_{II} mesophase. The explanation of its structure will be aided by revealing the ordering patterns, if such exist, of the GMO molecules. In the previous study (Kolev et al. 2014) (at higher temperature and in the absence of tricaprylin or cargo), enhanced ordering of GMO was registered both for the tails and for the headgroups. In order to check whether it has been influenced by the presence of tricaprylin or by the inclusion of the peptide, radial distribution functions of the GMO double bonds center-of-mass (COM) were generated and are presented in Fig. 12.

The obtained RDF curves show that the GMO structuring remains intact also in the presence of tricaprylin or lysozyme. Three peaks are clearly visible, which indicates relatively long-range ordering of the lipids. This implies that the peptide does not exert strong perturbation on the lipid structure in general. There is also no dependence of the RDF on the tube radii. However, several aspects of the lipid structure remain to be elucidated—how far-reaching the interaction between the lipids is, how collective the character of the ordering is, and does the presence of the peptide cause at least local perturbation on the GMO structuring. To elucidate these points, cross-correlation functions

Table 2 Numerical description of the packing frustration effect appearing in the H_{II} mesophase composed of GMO, tricaprylin, and water at 25 °C, without and with entrapped lysozyme

R_w (Å)	$L_{xy,min}$ (Å)	$L_{xy,max}$ (Å)	Δl_{xy} (Å)	l_{min} (Å)	l_{max} (Å)	Δl (Å)
Without entrapped lysozyme						
8.73	13.67	18.60	4.93	14.99	19.18	4.19
10.94	14.17	18.71	4.54	15.12	19.22	4.10
13.16	14.36	18.71	4.36	15.20	19.24	4.04
14.32	14.36	18.69	4.68	15.14	19.23	4.09
Average	14.05	18.68	4.63	15.11	19.22	4.11
With entrapped lysozyme						
10.81	13.84	18.56	4.72	15.06	19.16	4.10
12.30	13.69	18.54	4.85	14.97	19.18	4.21
13.51	13.66	18.44	4.78	14.95	19.13	4.18
Average	13.73	18.51	4.78	14.99	19.16	4.16

The most probable minimal and maximal GMO tail lengths are denoted with "min" and "max", estimated as the arguments of the inflection points in Fig. 11 (Chebyshev polynomials of degree 20 were employed to fit each curve). The average GMO tails layer thickness in the xy-plane, $\langle \Delta l_{xy} \rangle$, is a direct measure of the frustration effect and corresponds visually to the most populated part of the histograms (the one in red tones) in Fig. 6a. The absolute tail frustration estimator $\langle \Delta l \rangle$, based on the distribution of l, is given in the last column

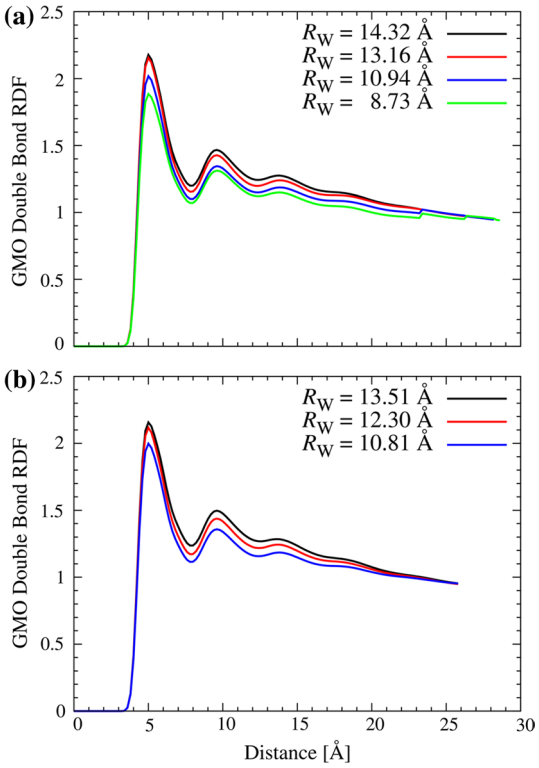

Fig. 12 Radial distribution functions (RDF) of the COM of GMO double bonds for the H_{II} mesophase incorporating tricaprylin without (**a**) and with (**b**) entrapped lysozyme

(CCFs) between the distances of GMO double bonds and their increase were generated and analyzed. Some illustrative results are presented in Fig. 13 and the methodology for obtaining the CCFs is described in Section S8 of the Supplementary Material.

The CCFs reveal some interesting trends. Their peak values do not exceed 0.25, which means that the GMO structuring does not correspond to a regular lattice. However, the decay of the cross-correlation functions is very slow in all cases, which signifies that the positions of the lipids are strongly influenced by those of the other GMO molecules, the effect often extending well beyond 100 molecules separation. This corroborates the information obtained from the RDF profiles and shows collective character of the GMO ordering. There is no strict dependence of the correlation on the tube diameter. The presence of lysozyme has some structure-breaking influence only in the narrowest tube. There, the maximum correlation decreases to ca. 0.1. Nevertheless, the CCFs decay in all peptide-filled systems becomes even slower. This implies that the lipid–lipid ordering range even extends, but this could merely be due to the longer simulation boxes and not to the biomolecule.

Water mobility

The *scalar* self-diffusivity of water molecules in the H_{II} mesophase, D, is obtained by tracking their mean-squared

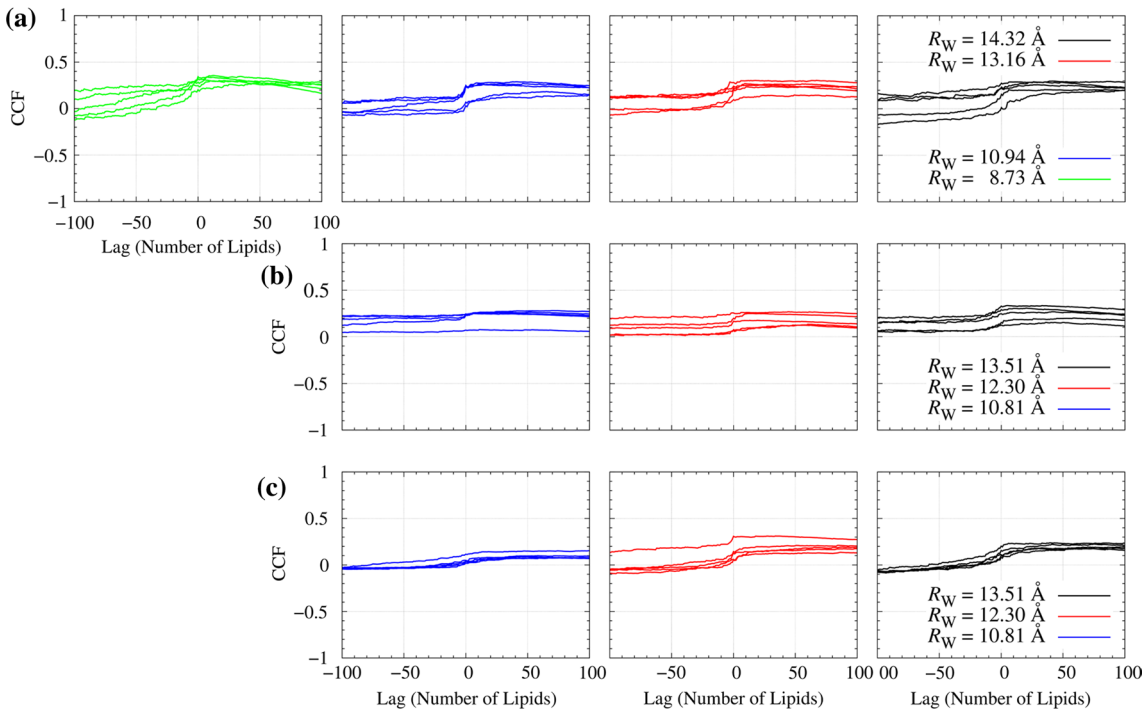

Fig. 13 Cross-correlation functions of the distance between the COMs of GMO double bonds for the H_{II} mesophase incorporating tricaprylin without entrapped lysozyme (**a**), and with entrapped lysozyme, where the lipids are far from (**b**) or close to (**c**) the peptide molecule; *different curves* correspond to different reference lipid molecules selected randomly within the respective region of the tubes

Table 3 The scalar self-diffusion coefficient of the water molecules, D, and its standard deviation for the H_{II} mesophase composed of GMO, tricaprylin, and water at 25 °C, without and with entrapped lysozyme

R_w (Å)	D [$\times 10^{-6}$ cm^2/s]
Without entrapped lysozyme	
8.73	2.975 ± 0.209
10.94	4.833 ± 0.181
13.16	6.918 ± 0.192
14.32	8.094 ± 0.219
With entrapped lysozyme	
10.81	3.501 ± 0.341
12.30	3.407 ± 1.450
13.51	3.041 ± 1.591

displacement (MSD). The self-diffusion tensor, $\boldsymbol{D}$, is diagonally predominant for all systems listed in Table 1, and the scalar D (Table 3) should be taken as $D = D_{xx} + D_{yy} + D_{zz} \approx D_{zz}$, where D_{xx}, D_{yy}, and D_{zz} are the diagonal elements of $\boldsymbol{D}$.

Due to the finite unique length of the simulation box and the relatively short simulation times, the values of D given in Table 3 for the system with uninterrupted water channel might be slightly underestimated (In-Chul and Hummer 2004).

For the H_{II} mesophase with entrapped lysozyme Table 3 shows that D coincides within the standard deviations. However, the latter are much larger than those for the systems without lysozyme. This means that the diffusion of water in the peptide-filled tubes is much more inhomogeneous and significantly depends on the length of the simulation box, L. Since the lysozyme molecules act as stoppers limiting the water molecules displacement in z-direction, meeting them lowers the water mobility and D and this becomes more probable in the wider tubes.

The role of diffusing water for hydrating lipid headgroups is analyzed in Section S9 of the Supplementary Material and its participation into hydrogen bonding with GMO headgroups—in Section S10 of the Supplementary Material.

Secondary structure of lysozyme

So far, only the structural characteristics of the H_{II} mesophase have been discussed. However, it is important to also assess the influence of the entrapment on the peptide molecule because preserving its secondary structure (SS) is important for the bioactivity after delivery. Therefore, the secondary structure of lysozyme [both in the GMO tubes and in aqueous solution) was quantified by DSSP analysis (Kabsch and Sander 1983 (Table 4)].

First, it is evident that during the MD simulation in aqueous solution, the SS remains very close to the one of the crystallographic geometry. Entrapment of lysozyme into the GMO tubes, however, causes significant perturbation of its secondary structure. In all cases the molecule becomes more disordered, which is evidenced by the increased share of the coil conformation. This comes at the expense of less β-sheet, β-bridge and α-helix regions. Especially the helical arrangement is disturbed systematically upon decrease of the tube diameter. The smallest mean absolute deviation of 4.75 % from the solution structure is registered for the tube with $R_w = 12.30$ Å, which shows that there is an optimum size of the channel, in which the SS undergoes the least disruption.

These results suggest that the enzyme will require some time for relaxation after release in order to be able to perform its regular activities in the organism. Given its small size and the fact that the structural changes are not dramatic, it is expected that this relaxation will not be too severe to prevent the peptide from functioning.

NVT vs. NPT simulations

Following the approach adopted in our previous study, we verified that the numerical results obtained by means of NVT and NPT simulations do not differ statistically also here. The results show that the NVT simulations neither

Table 4 Results from the DSSP analysis of the secondary structure (SS) of lysozyme from the PDB, in aqueous solution, and after insertion into GMO–TAG–water tubes; the second column contains the percentage of residues from the entire trajectory to which regular secondary structure (α-helix + β-sheet + β-bridge + turn) could be assigned and the subsequent columns list by what contributions of the various types of spatial arrangement of the amino acid residues it was formed; 6 ns trajectory was analyzed for free lysozyme and 60 ns fragments—for the confined one; all values are in %

Model	Regular SS	α-helix	β-sheet	β-bridge	Turn	3-helix	Bend	Coil
PDB (1AKI)	68	30	6	5	27	11	5	16
LYS–WAT	66	32	7	4	23	6	12	16
$R_w = 10.81$ Å	53	16	5	3	30	6	17	24
$R_w = 12.30$ Å	58	22	6	2	28	4	14	24
$R_w = 13.51$ Å	48	28	0	1	19	5	20	27

accumulate mechanical tension inside the GMO layer, nor keep the simulated system entrapped into some local minimum of the potential or total energy. The length of the trajectories was also tested by extending the simulations for two of the lysozyme-filled tubes up to 1.2 μs. This did not lead to any appreciable structural or dynamic changes, which coincides with findings by other authors (Kocherbitov 2015) that relatively short trajectories are sufficient to describe the systems of interest. Details are given to the interested readers in Section S11 of the Supplementary Material.

Conclusions

Molecular dynamics simulations of models of the inverted hexagonal mesophase of GMO stabilized by tricaprylin were carried out. The effect of loaded peptide cargo was analyzed. The primary focus was elucidation of the lipid structuring at the molecular level but the influence of the encapsulation on the peptide conformation was monitored, too.

The main observation is that the presence of tricaprylin molecules is essential for successful packing of GMO tails across the tubes. It is achieved by formation of tricaprylin "islands" among the GMO molecules. The net result is that the thermodynamically stable cylindrical shape of the water channel is stabilized even at room temperature where no pure GMO H_{II} mesophase can be formed. The individual molecular characteristics of the lipid molecules, such as hydrogen bonding between the lipid headgroups and water, radial distribution functions of the distances between GMO double bonds, or packing frustration of GMO tails are not affected drastically upon introduction of tricaprylin. It is established that although no regular lattice is formed by the GMO molecules, long-range ordering takes place, extending beyond 100 lipid molecules along the tubes axis. The properties of the systems do not vary materially with the tube diameter.

Entrapment of the lysozyme peptide induces local perturbation in the lipid structure but does not affect the behavior of the model systems in general. The mass distribution maps offer detailed information on the location and global orientation of the biomolecule. The secondary structure of the peptide is affected by the insertion and optimum radius of the lipid tubes should be sought, which minimizes the perturbation.

Acknowledgments Vesselin Kolev would like to acknowledge and extend his heartfelt gratitude to Technion for the provided partial fellowship. G. M. and A. I. are grateful to the European Union Framework Programme 7 project Beyond Everest. The authors want to express their thanks to Mr. Zdravko Zdravkov (Master in Arts) for helping make the graphics easier to digest.

References

Aherne M, Lyons JA, Caffrey M (2012) A fast, simple and robust protocol for growing crystals in the lipidic cubic phase. J Appl Crystallogr 45:1330–1333

Alfutimie A, Curtis R, Tiddy GJT (2015) The phase behaviour of mixed saturated and unsaturated monoglycerides in water system. Colloids Surf A 465:99–105

Amar-Yuli I, Garti N (2005) Transitions induced by solubilized fat into reverse hexagonal mesophases. Colloids Surf B 43:72–82

Amar-Yuli I, Azulay D, Mishraki T, Aserin A, Garti N (2011) The role of glycerol and phosphatidylcholine in solubilizing and enhancing insulin stability in reverse hexagonal mesophases. J Colloid Interface Sci 364:379–387

Artymiuk PJ, Blake CC, Rice DW, Wilson KS (1982) The structures of the monoclinic and orthorhombic forms of hen egg-white lysozyme at 6 Å Resolution. Acta Crystallogr Sect B: Struct Crystallogr Cryst Chem 38:778–783

Bayly C, Cieplak P, Cornell W, Kollman P (1993) A well-behaved electrostatic potential based method using charge restraints for deriving atomic charges: the RESP model. J Phys Chem 97:10269–10280

Bekker H, Berendsen HJC, Dijkstra EJ, Achterop S, van Drunen R, van der Spoel D, Sijbers A, Keegstra H, Reitsma B, Renardus MKR (1993) In: de Groot RA, Nadrchal J (eds) Proceedings of the 4th international conference physics computing '92. World Scientific, Singapore, pp 252–256

Berendsen HJC, van der Spoel D, van Drunen R (1995) GROMACS: a message-passing parallel molecular dynamics implementation. Comput Phys Commun 91:43–56

Cieplak P, Cornell W, Bayly C, Kollman P (1995) Application of the multimolecule and multiconformational RESP methodology to biopolymers: charge derivation for DNA, RNA, and proteins. J Comput Chem 16:1357–1377

Di Gregorio GM, Mariani P (2005) Rigidity and spontaneous curvature of lipidic monolayers in the presence of trehalose: a measurement in the DOPE inverted hexagonal phase. Eur Biophys J 34:67–81

Efrat R, Shalev DE, Hoffman RE, Aserin A, Garti N (2008) Effect of sodium diclofenac loads on mesophase components and structure. Langmuir 24:7590–7595

Fehér A, Urbán E, Erős I, Szabó-Révész P, Csányi E (2008) Lyotropic liquid crystal preconcentrates for the treatment of periodontal disease. Int J Pharm 358:23–26

Feller SE, MacKerell AD (2000) An improved empirical potential energy function for molecular simulations of phospholipids. J Phys Chem B 104:7510–7515

Hamm M, Kozlov M (1998) Tilt model of inverted amphiphilic mesophases. Eur Phys J B 6:519–528

Hess B, Kutzner C, van der Spoel D, Lindahl E (2008) GROMACS 4: algorithms for highly efficient, load-balanced, and scalable molecular simulation. J Chem Theory Comput 4:435–447

Humphrey W, Dalke A, Schulten K (1996) VMD: visual molecular dynamics. J Mol Graph 14:33–38

ImageMagick—software suite to create, edit, compose, or convert bitmap images. http://www.imagemagick.org

In-Chul Y, Hummer G (2004) System-size dependence of diffusion coefficients and viscosities from molecular dynamics simulations with periodic boundary conditions. J Phys Chem B 108:15873–15879

Kabsch W, Sander C (1983) Dictionary of protein secondary structure: pattern recognition of hydrogen-bonded and geometrical features. Biopolymers 22:2577–2637

Klauda JB, Brooks BR, MacKerell AD, Venable RM, Pastor RW (2005) An ab initio study on the torsional surface of alkanes

and its effect on molecular simulations of alkanes and a DPPC bilayer. J Phys Chem B 109:5300–5311

Kocherbitov V (2015) Molecular dynamics simulations of liquid crystalline phases of dodecyltrimethylammonium chloride. J Mol Liq 210:74–81

Kolev V, Ivanova A, Madjarova G, Aserin A, Garti N (2012) Molecular dynamics approach to water structure of H_{II} mesophase of monoolein. J Chem Phys 136:074509

Kolev V, Ivanova A, Madjarova G, Aserin A, Garti N (2014) Unit cell structure of water-filled monoolein into inverted hexagonal (H_{II}) mesophase modeled by molecular dynamics. J Phys Chem B 118:5459–5470

Kulkarni CV, Wachter W, Iglesias-Salto G, Engelskirchen S, Ahualli S (2011) Monoolein: a magic lipid? Phys Chem Chem Phys 13:3004–3021

Libster D, Aserin A, Wachtel E, Shoam G, Garti N (2007) An H_{II} liquid crystal-based delivery system for cyclosporin A: physical characterization. J Colloid Interface Sci 308:514–524

Libster D, Aserin A, Garti N (2011) Interactions of biomacromolecules with reverse hexagonal liquid crystals: drug delivery and crystallization applications. J Colloid Interface Sci 356:375–386

Lindahl E, Hess B, van der Spoel D (2001) GROMACS 3.0: a package for molecular simulation and trajectory analysis. J Mol Model 7:306–317

Luzzati V, Husson F (1962) The structure of the liquid-crystalline phases of lipid-water systems. J Cell Biol 12:207–219

Michaud-Agrawal N, Denning EJ, Woolf TB, Beckstein O (2011) MDAnalysis: a toolkit for the analysis of molecular dynamics simulations. J Comput Chem 32:2319–2327

Mishraki T, Libster D, Aserin A, Garti N (2010a) Temperature-dependent behavior of lysozyme within the reverse hexagonal mesophases (H_{II}). Colloids Surf B 75:391–397

Mishraki T, Libster D, Aserin A, Garti N (2010b) Lysozyme entrapped within reverse hexagonal mesophases: physical properties and structural behavior. Colloids Surf B 75:47–56

van der Spoel D, Lindahl E, Hess B, Groenhof G, Mark AE, Berendsen HJC (2005) GROMACS: fast, flexible and free. J Comput Chem 26:1701–1718

Zabara A, Mezzenga R (2012) Plenty of room to crystallize: swollen lipidic mesophases for improved and controlled in-meso protein crystallization. Soft Matter 8:6535–6541

Zabara A, Mezzenga R (2013) Modulating the crystal size and morphology of in meso-crystallized lysozyme by precisely controlling the water channel size of the hosting mesophase. Soft Matter 9:1010–1014

Zabara A, Amar-Yuli I, Mezzenga R (2011) Tuning in-meso-crystallized lysozyme polymorphism by lyotropic liquid crystal symmetry. Langmuir 27:6418–6425